

## Article

# Spectroscopic Measurement of Methylene Blue Distribution in Organs and Tissues of Hamadryas Baboons during Oral Administration

Elizaveta I. Kozlikina <sup>1,2,\*</sup> , Daria V. Pominova <sup>1</sup>, Anastasia V. Ryabova <sup>1</sup> , Kanamat T. Efendiev <sup>1,2</sup>, Aleksei S. Skobeltsin <sup>1,2</sup>, Natalia S. Rudenko <sup>3</sup>, Olga G. Kulik <sup>3</sup>, Evgeniya I. Muhametzyanova <sup>3</sup>, Dzina D. Karal-ogly <sup>3</sup>, Gleb A. Zhemerikin <sup>4</sup>, Dmitry V. Bulgin <sup>3</sup> , Artem A. Shiryaev <sup>4</sup>, Igor V. Reshetov <sup>4</sup> and Victor B. Loschenov <sup>1,2</sup>

- <sup>1</sup> Prokhorov General Physics Institute of the Russian Academy of Sciences, 119991 Moscow, Russia; pominovadv@nsc.gpi.ru (D.V.P.); nastya.ryabova@nsc.gpi.ru (A.V.R.); efendiev.kt@nsc.gpi.ru (K.T.E.); skobeltsin.as@nsc.gpi.ru (A.S.S.); loschenov@nsc.gpi.ru (V.B.L.)
- <sup>2</sup> Institute for Physics and Engineering in Biomedicine, National Research Nuclear University MEPhI, 115409 Moscow, Russia
- <sup>3</sup> Federal State Budgetary Scientific Institution "Research Institute of Medical Primatology", 354375 Sochi, Russia; lab-rms@mail.ru (N.S.R.); giz-olga69@mail.ru (O.G.K.); evg.m89@mail.ru (E.I.M.); karal\_5@mail.ru (D.D.K.); molmed1999@yahoo.com (D.V.B.)
- <sup>4</sup> Levshin Institute of Cluster Oncology, University Clinical Hospital No. 1, Sechenov First Moscow State Medical University (Sechenov University) Ministry of Health of the Russian Federation, 119146 Moscow, Russia; zhemerikin\_g\_a@staff.sechenov.ru (G.A.Z.); shiryaev\_a\_a@staff.sechtnov.ru (A.A.S.); reshetov\_i\_v@staff.sechenov.ru (I.V.R.)
- \* Correspondence: kozlikina.ei@nsc.gpi.ru



**Citation:** Kozlikina, E.I.; Pominova, D.V.; Ryabova, A.V.; Efendiev, K.T.; Skobeltsin, A.S.; Rudenko, N.S.; Kulik, O.G.; Muhametzyanova, E.I.; Karal-ogly, D.D.; Zhemerikin, G.A.; et al. Spectroscopic Measurement of Methylene Blue Distribution in Organs and Tissues of Hamadryas Baboons during Oral Administration. *Photonics* **2021**, *8*, 294. <https://doi.org/10.3390/photonics8080294>

Received: 11 June 2021  
Accepted: 21 July 2021  
Published: 24 July 2021

**Publisher's Note:** MDPI stays neutral with regard to jurisdictional claims in published maps and institutional affiliations.



**Copyright:** © 2021 by the authors. Licensee MDPI, Basel, Switzerland. This article is an open access article distributed under the terms and conditions of the Creative Commons Attribution (CC BY) license (<https://creativecommons.org/licenses/by/4.0/>).

**Abstract:** New research on Methylene Blue (MB), carried out in 2020, shows that it can be an effective antiviral drug as part of COVID-19 treatment. According to the research findings, MB has potential as a direct antiviral drug for the prevention and treatment of COVID-19 in the first stages of the disease. However, the MB accumulation by various types of tissues, as well as by immune cells, has not been previously studied. Therefore, the objective of this study was to obtain spectral data on the interstitial distribution of the administered drug in endothelial tissues in primates. The data on interstitial MB distribution obtained by spectroscopic measurement at both macro- and microlevels during oral administration to Hamadryas baboon individuals demonstrate that MB accumulates in mucous membranes of gastrointestinal tract and the tissues of the respiratory, cardiovascular, immune, and nervous systems. Additionally, it was found that MB was present in lung and brain myeloid cells in significant concentrations, which makes it potentially useful for protection from autoimmune response (cytokine storm) and as a tool for the correction of immunocompetent cells' functional state during laser irradiation. Since the cytokine storm starts from monocytic cells during SARS-CoV-2 cellular damage and since tumor-associated macrophages can significantly alter tumor metabolism, accumulation of MB in these cells provides a reason to conclude that the immune response correction in COVID-19 patients and change in macrophages phenotype can be achieved by deactivation of inflammatory macrophages in tissues with MB using laser radiation of red spectral range.

**Keywords:** methylene blue; photosensitizer delivery; COVID-19; PDT

## 1. Introduction

MB is a thiazine dye that is extensively used in various fields of science. MB is a well-known low-toxic biocompatible material. It has been shown that MB is not carcinogenic within the dose <2 mg/kg [1,2]. Clinically, MB is used in methemoglobinemia [3], malaria [4], hepatitis virus, and Alzheimer's disease treatment [5,6]. MB solutions are injected intravenously for cyanide, carbon monoxide, and hydrogen sulfide poisonings [7,8]. MB had been used in psychiatry as well [9]. It was administered in doses from 15 to 300 mg

daily, and the maximum concentration of MB in the blood was registered within 1 to 2 h after administration. However, it was not shown what the effective dose and blood concentration for psychiatric indications should be. In addition, patients who used serotonin re-uptake inhibitors experienced serotonin toxicity after MB intravenous injection [10].

The possibilities of MB application are caused by its redox properties. During methemoglobinemia (primary or developed as a result of poisoning), up to 20–50 % of all hemoglobin is present in the methemoglobin form, in which iron is trivalent. Methemoglobin cannot be an oxygen carrier from the lungs to tissues; hence, during its generation in considerable quantities, a decline in blood oxygen content occurs, and the transporting function of blood is inhibited. For methemoglobinemia treatment, the MB ability to change from its reduced form—leucomethylene blue (LMB)—into its oxidized form, by converting iron from trivalent to bivalent, is used.

Likewise, MB fluoresces in the red part of the spectrum and is photodynamically active. It is one of the basic photosensitizers (PS) for carrying out fluorescent diagnostics [11–13] and producing singlet oxygen within conduction of photodynamic therapy (PDT) in oncological disease treatment [14,15]. As recent studies have shown, during photoaction, MB has an outstanding antiviral effect toward Ebola virus and coronavirus MERS-CoV in plasma [16–18].

Despite having a wide scope of application and high potential, the MB ability to be an acceptor and LMB to be a donor of hydrogen in an organism and the mechanisms of its operating principles within the human body, during photoexcitation in particular, remain poorly understood.

The most frequent types of MB administration are intravenous injection and oral administration. According to Peter *et al.* [19], during intravenous injection to rats, the MB accumulation in the central nervous and cardiovascular systems reached a maximum value that could lead to a serotonin syndrome when using high concentrations of the drug [10,20]. In addition, Peter C. *et al.* [19] showed that on quarter of MB is eliminated via the kidneys, and three quarters of LMB. During oral administration, the MB accumulation in the walls of gastrointestinal tract and urinary system was the highest. The pharmacokinetics and pharmacodynamics of MB in other body systems remain unexplored to date.

The change in MB spectroscopic properties during its reduction or oxidation is of considerable importance. Reduction of MB turns it into LMB. Each form of drug has its absorbance peaks: LMB predominantly absorbs in UV region (256 nm), while MB has two absorbance peaks in UV and visible regions (294 and 665 nm, respectively) [21]. The MB absorption spectrum is presented on Figure 1.

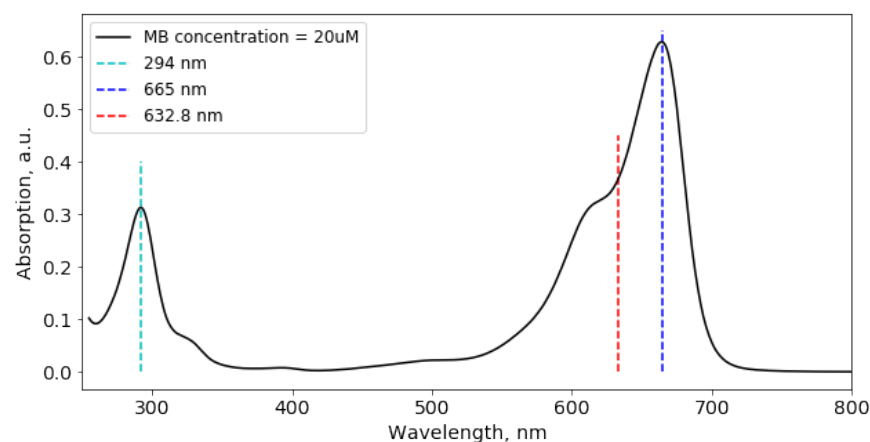


**Figure 1.** Absorption spectrum of MB.

The transition between drug forms can be done in several ways:

- By transferring one hydride anion, for example, from nicotinamide adenine dinucleotide (NADH) or dihydroflavine adenine dinucleotide (FADH<sub>2</sub>) or an appropriate substrate, MB passes into LMB.
- During dehydrogenation, LMB can transform into MB during the reduction of iron from trivalent form (MHb) to bivalent form (Hb) in erythrocyte cells and in the presence of oxygen.

In addition, MB has its separate cycle of work as a PS. Upon excitation of the drug by a source of laser light with a wavelength within the absorption band of MB, the MB molecule from the ground state (MB<sup>0</sup>) transitions into an excited singlet state (MB<sup>1</sup>), and then into a triplet state (MB<sup>3</sup>). During the collision of MB<sup>3</sup> and oxygen, energy transfer occurs, in which MB<sup>3</sup> returns to the ground state, thereby transferring oxygen to the singlet state (<sup>1</sup>O<sub>2</sub>) and other reactive oxygen species (ROS) that can destroy nearby biomolecules (Figure 2).

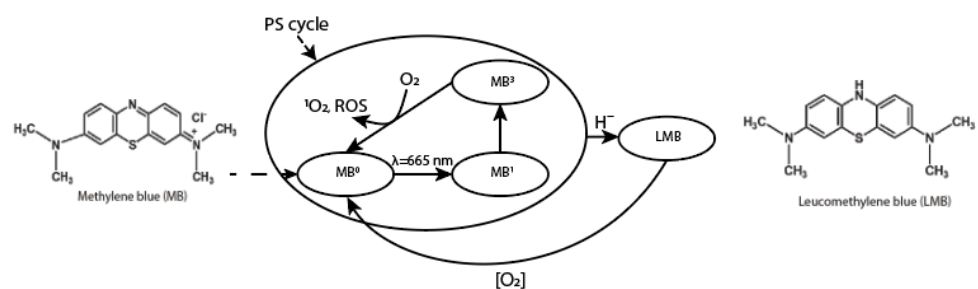


**Figure 2.** A simplified diagram of MB working in the human body.

The uniqueness of the PDT method is based on the cellular response induction to biological structures damage by ROS—natural regulators of cell proliferation, metabolism, and apoptosis. As a result of PDT, mediators that provoke a local inflammatory reaction and cytotoxic activity of immunocompetent cells in relation to the oncological disease are released.

Likewise, MB functions as an alternative electron carrier in mitochondria, which accepts electrons from NADH or FADH<sub>2</sub> and transfers them to coenzyme Q10 (CoQ) or cytochrome-c (Cyt-c), bypassing complex I/III blocking (Figure 3) [22]. In addition, McDonagh E.M et al. showed that the mechanism of action of MB is dependent on the intracellular capacity for NADP/NADPH recycling [23].

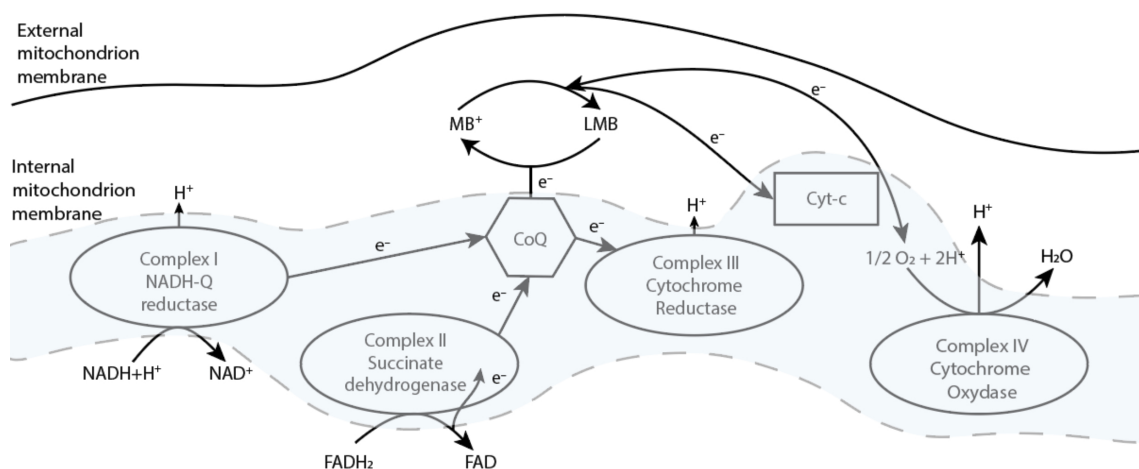


**Figure 3.** MB as a carrier of electrons in the electron transport chain inside the mitochondrion.

MB can also influence various cell signaling pathways. According to published studies, MB inhibits the activation of inflammasomes that induce the maturation of interleukins IL-1 $\beta$  and IL-18, as well as caspase-1 mediated cell death known as pyroptosis. In addition,

MB inhibits the upstream signals of anti-inflammatory assembly, phagocytosis, and gene expression of inflammatory components by inhibiting NF- $\kappa$ B signaling. It was also found that MB reduces the activity of caspase-1 [24]. In a drug product based on MB, the description in [25] mentions that MB is metabolized by CYPs 1A2, 2C19, and 2D6 in vitro; however, the predominant in vitro pathway appears to be UGT-mediated conjugation by multiple UGT enzymes, including UGT1A4 and UGT1A9. Approximately 40% of methylene blue is excreted into the urine unchanged.

During the last year, two clinical trials (phase I and phase II) of MB usage against COVID-19 have been started [26,27]. Alamdari D.H. et al. the reduced form of MB (mixture of MB, vitamin C, and N-acetyl cysteine) in the treatment of critically ill patients, while Ticino, F.E. et al. used the basic MB form for COVID-19 treatment.

New MB studies conducted in 2020 showed it may be as effective as a preventive treatment for COVID-19 [18,26]. The preventive effect is due to the fact that MB blocks the ACE2 receptors, which play one of the main roles in the penetration of SARS-CoV-2 into cells of predominantly endothelial origin [28]. In this regard, the localization, degree of accumulation, and MB elimination from endothelial tissues are of great interest. Thus, if MB accumulates in the surface layers of organs in concentrations sufficient for protection, then their protection from SARS-CoV-2 seems possible.

The MB accumulation by various types of tissues, as well as by immune cells, has not been previously studied. Therefore, the aim of this study was to obtain spectral data on the interstitial distribution of the administered drug in endothelial tissues in primates. This is important for assessing the MB protective properties against COVID-19, to perform effective PDT as well as to change macrophage polarization towards the pro-inflammatory response of immunity to tumor cells. The drug accumulation in organs and tissues was assessed by the intensity of luminescence upon excitation at a wavelength of 632.8 nm using a fiber-optic spectrometer. The study of MB distribution in organs and tissues at the microlevel was carried out using laser scanning confocal microscopy, which made it possible to estimate the concentration of the drug in various layers of the studied tissues, as well as in individual cells.

## 2. Materials and Methods

### 2.1. Regulations and Hamadryas Baboons Study of MB Distribution

All experiments involving animals were performed in accordance with the ethical standards set forth in the 1964 Helsinki Declaration and its subsequent amendments, approved by bioethics committee from the Research Institute of Medical Primatology (ethical commission approval protocol 67/A), and carried out at the same Institute. The drug distribution in organs and tissues of experimental animals, primates of the Hamadryas baboon species, was investigated (Table 1).

**Table 1.** Parameters of the experimental animals.

Identification Number	#	Age, y.o.	Body Weight, kg	Sex	t <sup>a</sup> , h
45247	A	2	1.5	M	3
41760	B	6	2.5	M	24
41086	C	7	2.5	M	0 (negative control)

<sup>a</sup> Time of MB accumulation.

The choice of experimental animals was based on primates similarity to humans in aspects of anatomy and physiology of specific organ systems. In addition, the results of studies demonstrated on small laboratory animals do not give a picture of the PS and light fluxes distribution with the required degree of accuracy, given the significant difference in the geometric dimensions of the tissues under study and the fiber-optic device structure. In addition, the results of such a study can easily be translated into clinical trial protocols.

The study was carried out over two days. For two primates from the group (A and B), the drug was orally administered once at a dose of 5 mg/kg. For the third primate (C),

selected as a negative control, ordinary water in the same volume was orally administered. The concentration administered to primates was selected based on the weight of the animals, the average weight of a person, and the MB safe dose administered to a person [29]. The concentration conversion is shown below (Formula (1)):

$$EAD = EHD \cdot \left( \frac{M_{human}}{M_{animal}} \right)^{0.33} \quad (1)$$

where  $EAD$  is the equivalent animal dose,  $EHD$  is the equivalent human dose that equals 1.5 mg/kg,  $M_{human}$  is the average human mass that equals 70 kg, and  $M_{animal}$  is the average primate mass that equals 2 kg.

Euthanasia of Primates A and C was performed 3 h after the start of the experiment, and of Primate B 24 h after the start of the experiment. Necropsy of the corpses of all animals was performed with complete organo-complex evisceration. The external state of the body, natural anatomical openings, brain, organs of the thoracic and abdominal cavities, pelvic organs, neck with organs and tissues, and musculoskeletal system were examined.

## 2.2. Registration of MB Fluorescence Spectra in Organs and Tissues Using a Fiber-Optic Spectrometer

To register the fluorescent signal, a LESA-01-BIOSPEC spectrometer (Biospec, Russia) was used (Figure 4). For registration and analysis of spectral dependencies, UnoMomento software (Biospec, Russia) was used with additional functions to account for absorbing and scattering properties. The device allows measurements of fluorescence spectra in the 350–1000 nm wavelength range with a 3 nm resolution. The exposure time for registration of one spectrum can be varied within the range of 20–500 ms.

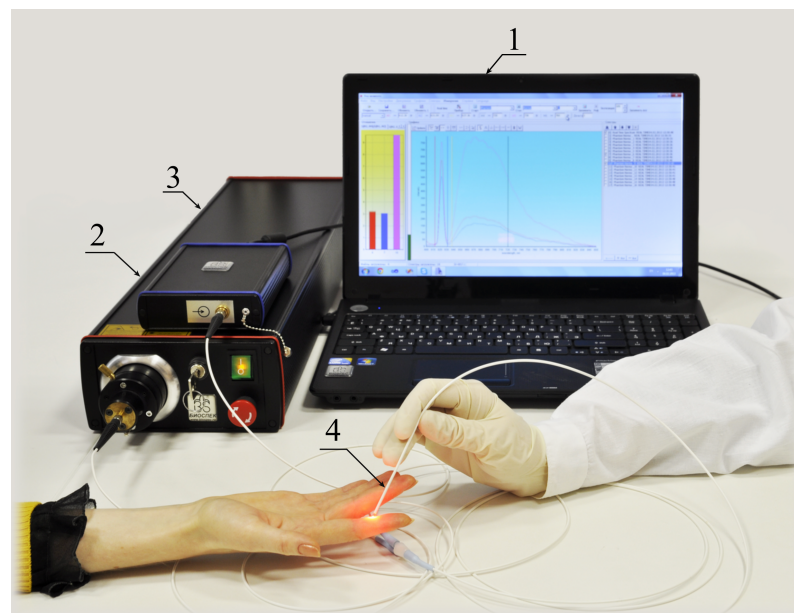


**Figure 4.** Scheme of a system for measuring fluorescence spectra *in vivo*: (1) PC with installed software; (2) spectrometer; (3) laser light source; (4) Y-shaped fiber-optic probe.

A fiber-optic probe with a central illuminating fiber supplying exciting laser radiation or white light to the tissue and six peripheral fibers collecting scattered and fluorescent radiation is used. The optical fiber core diameter was 200  $\mu\text{m}$ .

A He-Ne laser with a wavelength of 632.8 nm was used to excite MB fluorescence to separate excitation laser radiation and MB fluorescence. The laser power at the fiber exit was 5 mW. At the entrance to the spectrometer, a filter was installed that attenuated the laser radiation, which made it possible to observe its component backscattered by the tissue in the same dynamic range as the fluorescent radiation. The selective absorption colored glass optical filter according to customer requirements was specially developed

which suppresses 632.8 nm laser radiation signal  $10^3$ – $10^4$  times and transmits a fluorescent signal no worse than 70–90% in 640–900 nm diapason.

To quantitatively determine the MB concentration in organs and tissues, the fiber-optic spectrometer was calibrated using optical phantoms with a PS, simulating the scattering and absorbing properties of biological tissues. MB in various concentrations (0, 0.01, 0.05, 0.1, 0.5, 1, 2.5, and 5 mg/kg) was mixed with a scattering medium (1% MLT/LCT Intralipid) and poured into test tubes.

The fluorescence spectra of freshly prepared optical phantoms with MB were registered using the spectrometer and the laser source with a wavelength of 632.8 nm. On the basis of the obtained spectra, the fluorescence index was determined for each optical phantom. The average fluorescence index is calculated using the following formula:

$$\eta = \frac{\sum_n \frac{S_n(\text{fluorescence})}{S_n(\text{laserpeak})}}{n} \quad (2)$$

where  $n$  is the number of recorded spectra of one area,  $S_n(\text{fluorescence})$  is the integral of the selected area for MB fluorescence in the area under study, and  $S_n(\text{laserpeak})$  is the integral of the selected area of the laser peak.

The signal-to-noise ratio made it possible to establish a one-to-one correspondence between the fluorescence index of each of the phantoms and the MB concentration in it (Figure 5a). Fluorescent images of the investigated phantoms obtained using a black-and-white camera and an interference filter LONG PASS-650 are shown in Figure 5b. Determination of the fluorescence index and MB concentration in optical phantoms was carried out under the same external conditions. All measurements were carried out in a dark room without external light sources.

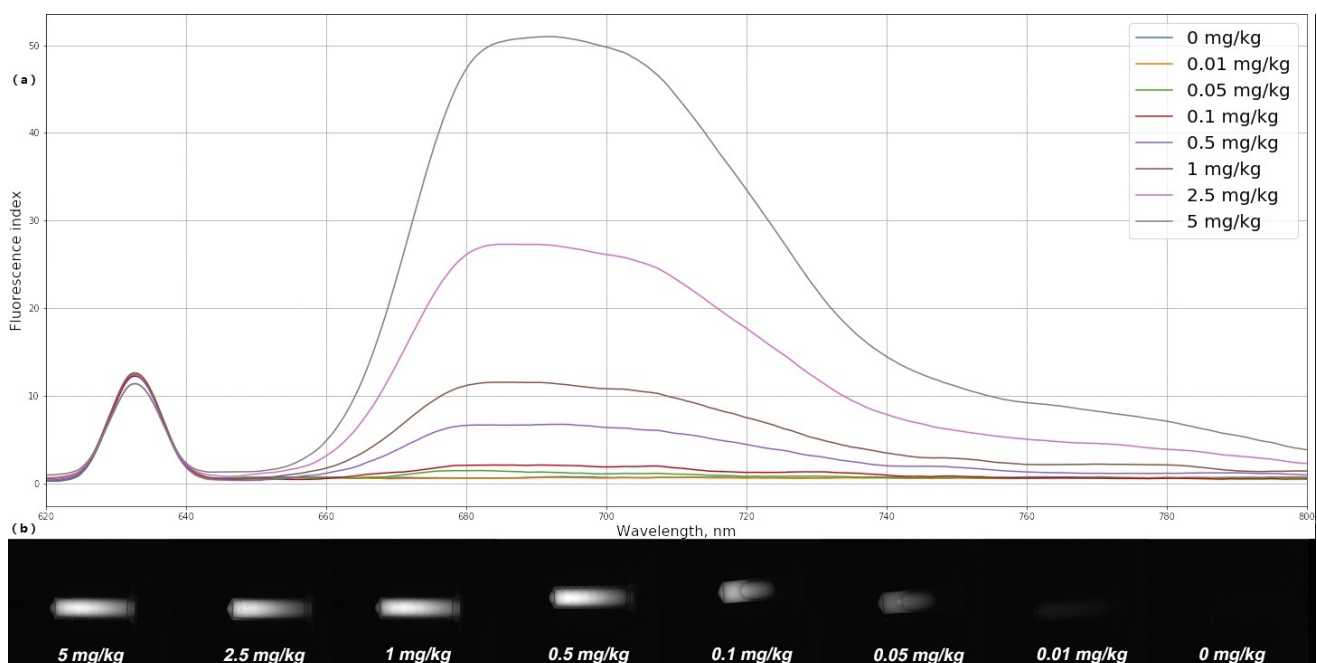


**Figure 5.** Fluorescence spectra of optical phantoms with MB photosensitizer at different concentrations (a); fluorescence images of optical phantoms with different MB concentrations obtained using a black-and-white camera and a filter (b).

Evaluation of the accumulation and determination of the drug concentration in the tissues using a fiber-optic spectrometer was carried out integrally from the entire depth to which the laser signal penetrates. Thus, using a fiber-optic spectrometer, the possibility of assessing the drug accumulation in a certain layer of biological tissue, for example, in the endothelium, is lost. For a more detailed assessment of the accumulation, a laser scanning confocal microscope was used.

### 2.3. Registration of MB Fluorescence Spectra in Organs and Tissues Using a Laser Scanning Confocal Microscopy. Immunofluorescence Analysis

#### 2.3.1. Fluorescence Study

The localization and the intensity of MB fluorescence in tissue cross sections was determined by using a laser scanning confocal microscope LSM-710-NLO (Carl Zeiss Microscopy, Jena, Germany).

The primate was euthanized and the tissue samples of interest were removed and fixed in 4% formalin. The fixed tissue pieces were blotted dry, mounted on a platform with Neg-50™ frozen section medium (Richard-Allan Scientific™, San Diego, CA, USA), and rapidly frozen at  $-26^{\circ}\text{C}$  directly in the chamber of microtome cryostat Microm HM 540 (Thermo Fisher Scientific Microm International GmbH, Kalamazoo, MI, USA).

Sections of frozen tissues were performed using the standard method: frozen cross sections,  $15\ \mu\text{m}$  thick, were placed on glass slides without any additional staining, air-dried, and mounted under a cover glass in glycerol.

Sections were analyzed immediately after preparation using 632.8 nm laser for MB fluorescence excitation and spectrally resolved image acquisition mode with 32-channel GaAsP detector in 650–730 nm range. To acquire the images, a  $20\times$  Plan-Apochromat (NA 0.8) lens was used.

The transmitted laser light was recorded with a T-PMT channel (photomultiplier tube for transmitted light).

MB optical phantoms in various concentrations (0, 0.01, 0.05, 0.1, 0.5, 1, 2.5, 5, 10, and 25 mg/kg) were used for laser scanning confocal microscopy calibration for quantitative analysis of MB concentration in organs and tissues of experimental animals. A drop of the phantom was placed on a cover glass and irradiated with a laser light source with a wavelength of 632.8 nm, after which fluorescence was observed at a wavelength of 685 nm (Figure 6). The fluorescence intensity was determined by the white-highlighted area on the drop. After calibration, a one-to-one correspondence was established between the fluorescence intensity and the MB concentration in the optical phantom.

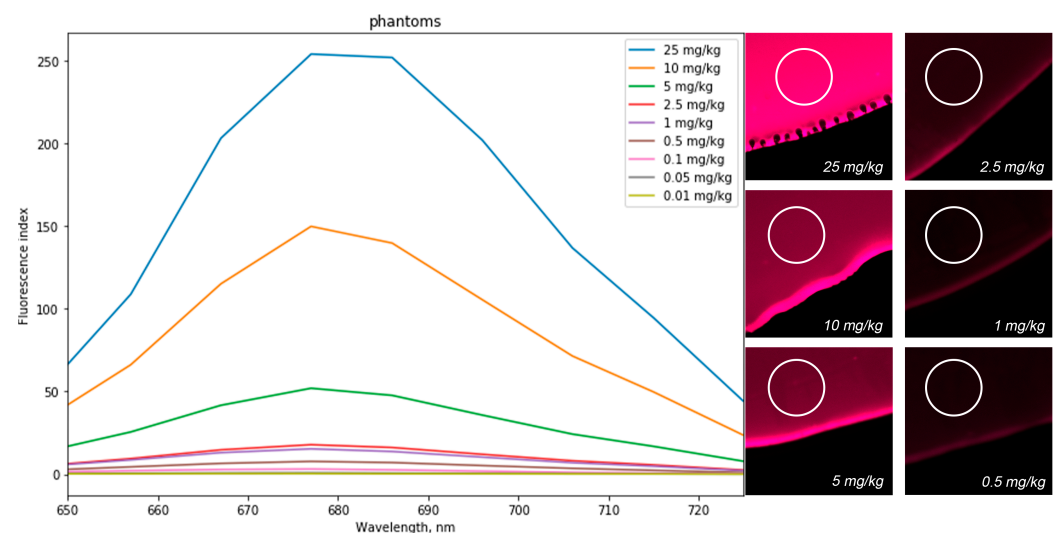


**Figure 6.** Fluorescence spectra of MB phantoms and images of phantom drops obtained by using laser scanning confocal microscopy.

#### 2.3.2. Immunofluorescence Analysis

Immunofluorescence analysis of two tissues types was performed according to the following protocol. Frozen cross sections,  $5\ \mu\text{m}$  thick, were mounted on superfrost plus slides. Sections were rinsed in PBS-TWEEN 20 two times for 2 min. Next, they were blocked by the NBCS (Newborn Calf Serum, 5%) solution. Sections were incubated with primary antibodies (anti-human CD86, isotype Mouse IgG1 diluted in 1% PBS-NBCS 1:100) in a

humid chamber at room temperature for 1 h. Sections were then incubated with secondary antibodies (Alexa Fluor 488 anti-mouse, isotype Rat IgG diluted in 1% PBS-NBCS 1:100) under the same conditions. Then, counterstain with Hoechst (diluted with PBS 1:2000) was performed. Finally, sections were coverslipped with glycerol medium.

Sections were analyzed immediately after preparation using a 632.8 nm laser source for MB excitation, 740 nm femtosecond laser Chameleon Ultra II (Coherent, Santa Clara, CA, USA) for Hoechst excitation and 488 nm Lasos laser source for Alexa Fluor 488 excitation. Sections of two types of tissues (lung and brain) were analyzed on the presence of myeloid cells.

### 3. Results

#### 3.1. Comparative Spectral Study of the Organs of Primates with the Administered MB after 3 and 24 Hours Using a Fiber-Optic Spectrometer

The MB fluorescence spectra in the organs of primates 3 and 24 h after oral administration were registered and the corresponding fluorescence indices for each organ were calculated (Formula (1) was used taking into account the subtraction of endogenous fluorescence obtained from the control Primate C). The histogram of the MB fluorescence indices, taking into account the indices of endogenous fluorescence by subtraction, in the organs of primates 3 (Primate A) and 24 h (Primate B) after oral administration of the drug are shown in Figure 7. Fluorescence indices corresponding to phantoms with known concentration are shown by dotted lines.

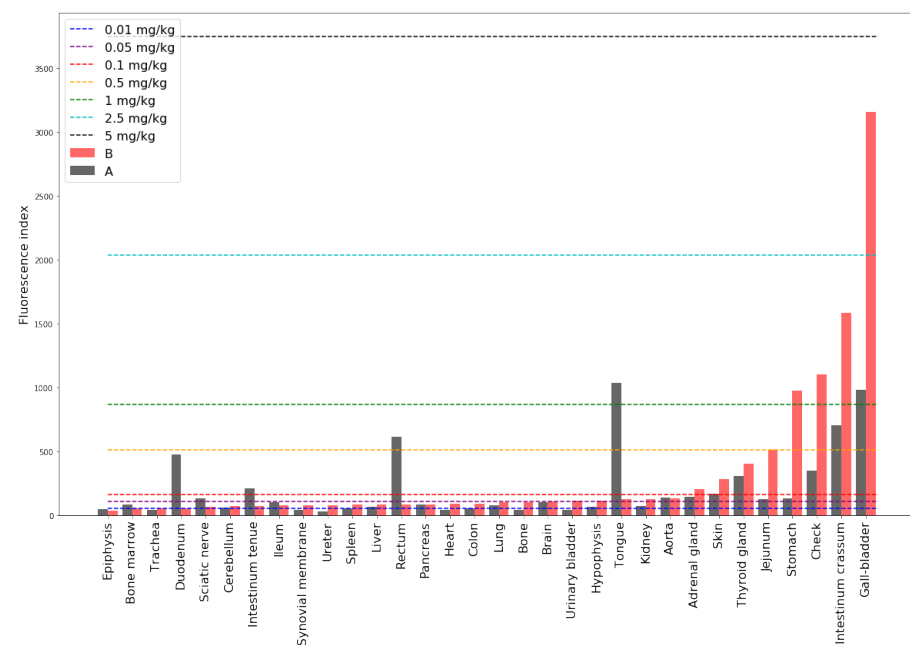


**Figure 7.** Fluorescence indices of organs of Primates A (3 h after administration) and B (24 h after administration). Fluorescence indices corresponding to phantoms with known concentration are shown by dotted lines.

The highest accumulation 3 h after administration of the drug was registered in the gallbladder, intestinum crassum, and stomach. Analysis of the fluorescence index time of drug accumulation dependence showed the following tendencies. In the majority of organs, MB concentration increased with time after injection. In organs of the digestive system such as the gallbladder, colon, liver, intestinum crassum, and stomach, the drug concentration was increased by a factor of 2, 2.4, 3.5, 4, and 14, respectively, the next day.

In organs of the endocrine system—thyroid, pancreas, and adrenal glands—MB accumulation was increased the next day by a factor of 1.3, 1.1, and 1.4, respectively. In addition, after 24 h, an increase in concentration was also observed in the organs of the urinary system—in the kidneys and ureter. The accumulation in the tissues of the cardiovascular and nervous systems also increased: in the cerebellum by 1.2 times,

in the hypophysis by 1.7 times, and in the heart by 2.3 times. An increase in the MB concentration in the synovial membrane and spleen was also observed. It is especially worth noting a significant increase in accumulation in the lungs and trachea (1.3 times). The MB accumulation in these organs is of great importance since these organs are the “targets” for SARS-CoV-2.

Exceptions in which a decrease in the MB concentration was observed with an increase in the accumulation time were: tongue, rectum, ileum, jejunum, sciatic nerve, duodenum, bone marrow, epiphysis, and aorta. This effect requires additional research.

### 3.2. Spectral Study of MB Accumulation in the Organs of Primates Using a Scanning Laser Confocal Microscope

During the post-mortem examination, organ specimens of greatest interest were taken for further study of the MB accumulation in endothelial tissues: jejunum, stomach, intestinum crassum, colon, gallbladder, liver, tongue, thymus, spleen, white and gray matter, cerebellum, ureter, aorta, kidney, pancreas, heart, and lungs. The organs of two primates were analyzed using laser scanning confocal microscopy to assess the drug accumulation in the thin layer of the sample (15  $\mu\text{m}$ ). Microscopic fluorescent images of the examined organs are shown in Figures 8 and 9 for Primate A and Figures 10 and 11 for Primate B. Areas of interest are highlighted in white, for which the accumulated concentration of MB was calculated. The fl index corresponds to the MB concentration in this area in terms of mg/kg.

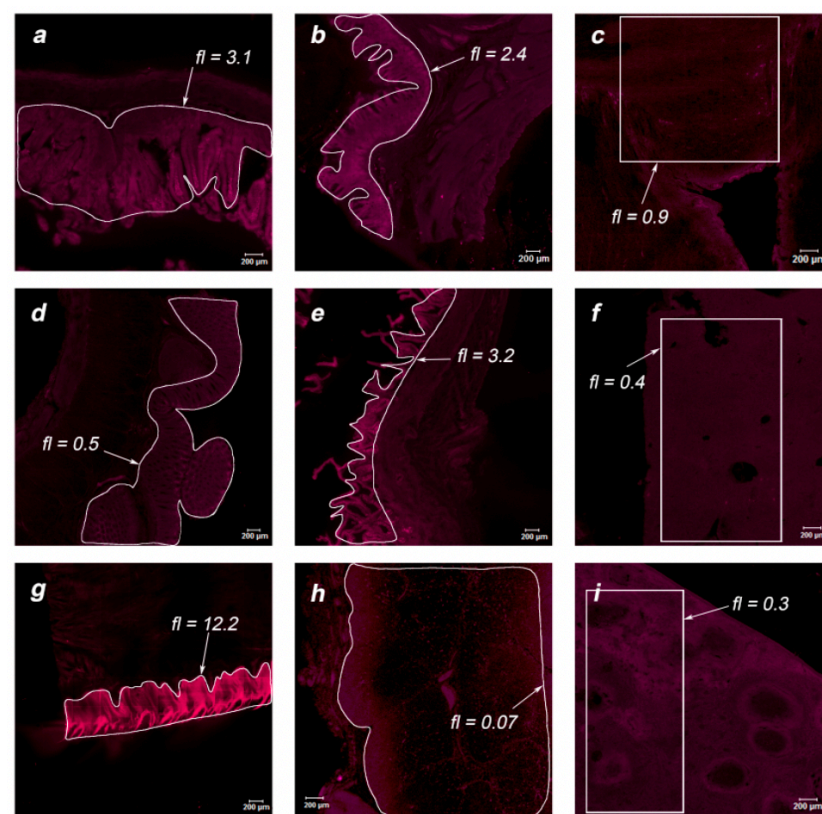


**Figure 8.** Images of organs of Primate A (3 h after MB administration) obtained using laser scanning confocal microscopy: (a) jejunum; (b) stomach; (c) intestinum crassum; (d) colon; (e) gallbladder; (f) liver; (g) tongue; (h) thymus; (i) spleen. Areas of interest are highlighted in white, according to the accumulated MB. The index corresponds to the level of MB in this area of mg/kg.

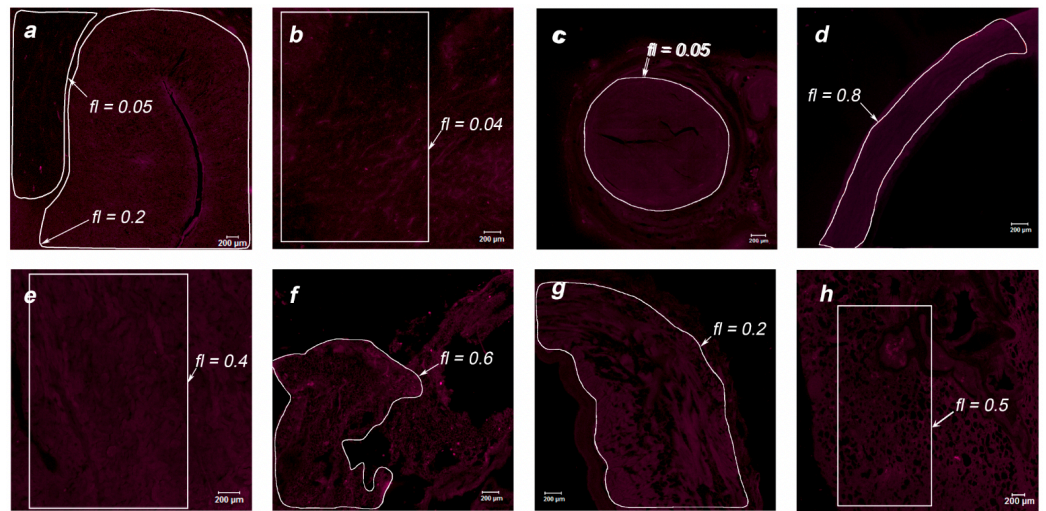


**Figure 9.** Images of organs of Primate A (3 h after MB administration) obtained using laser scanning confocal microscopy: (a) white and gray matter; (b) cerebellum; (c) ureter; (d) aorta; (e) kidney; (f) pancreas; (g) heart; (h) lungs. Areas of interest are highlighted in white, according to the accumulated MB. The index corresponds to the level of MB in this area of mg/kg.

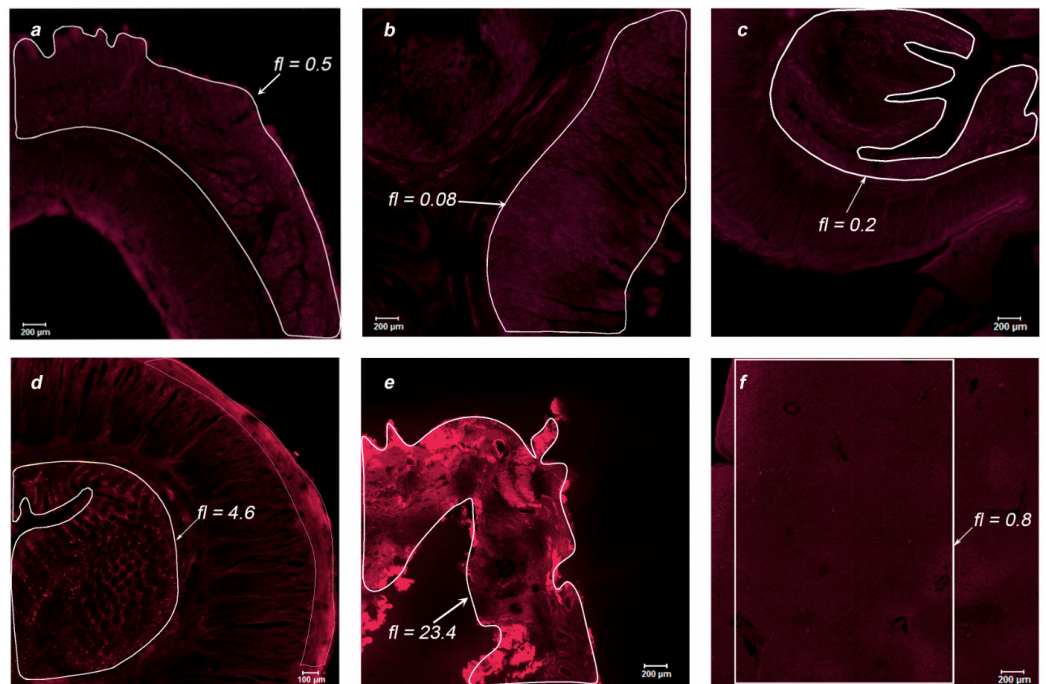


**Figure 10.** Images of organs of Primate B (24 h after MB administration) obtained using laser scanning confocal microscopy: (a) jejunum; (b) stomach; (c) intestinum crassum; (d) colon; (e) gallbladder; (f) liver. Areas of interest are highlighted in white, according to the accumulated MB. The index corresponds to the level of MB in this area of mg/kg.

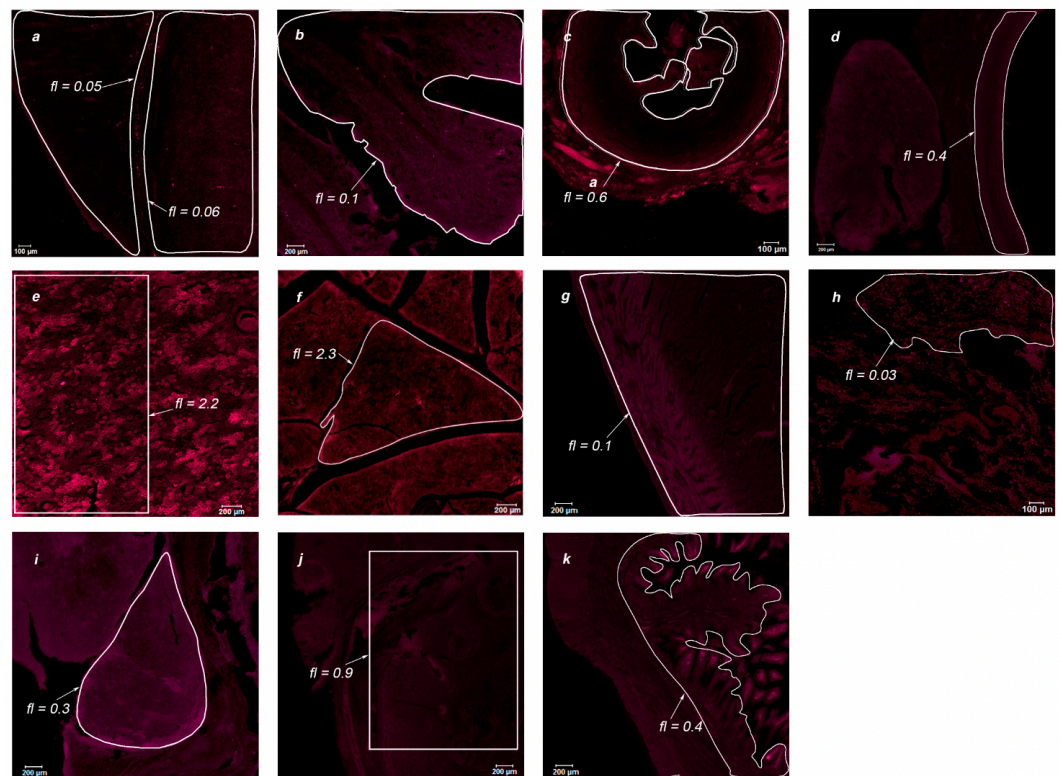


**Figure 11.** Images of organs of Primate B (24 h after MB administration) obtained using laser scanning confocal microscopy: (a) white and gray matter; (b) cerebellum; (c) ureter; (d) aorta; (e) kidney; (f) pancreas; (g) heart; (h) lungs; (i) hypophysis; (j) spleen; (k) ileum. Areas of interest are highlighted in white, according to the accumulated MB. The index corresponds to the level of MB in this area of mg/kg.

Within the digestive system of each primate, the maximum accumulation was observed in the internal endothelium of organs. In the tissues of the lungs and white and gray matter, an inhomogeneous distribution of MB is visible (bright points). To analyze these points, an immunofluorescence analysis was performed.

### 3.3. Immunofluorescence Analysis

Since myeloid cells are directly involved in the immune response after PDT, two types of tissues (lungs and white and gray matter) of Primates A–C (Primate C is the control) were analyzed for the presence of myeloid cells and their MB accumulation. Microscopic fluorescent images of cryosections after immunofluorescent staining are shown in Figure 12.

The obtained images show myeloid cells expressing CD86 (indicated by arrows).

In the results presented above, the organs of two primates were examined after oral administration of MB after 3 and 24 h, respectively, by using both a laser scanning confocal microscope to assess the accumulation of the drug in the thin layer of the sample and a fiber-optic spectrometer to evaluate the average accumulation of the drug over the entire depth of the investigated organ, into which the laser light penetrates. Thus, it is possible to compare the evaluated MB accumulation in the same organs using different research methods and identify the most suitable approach for the set goals (Figure 13).

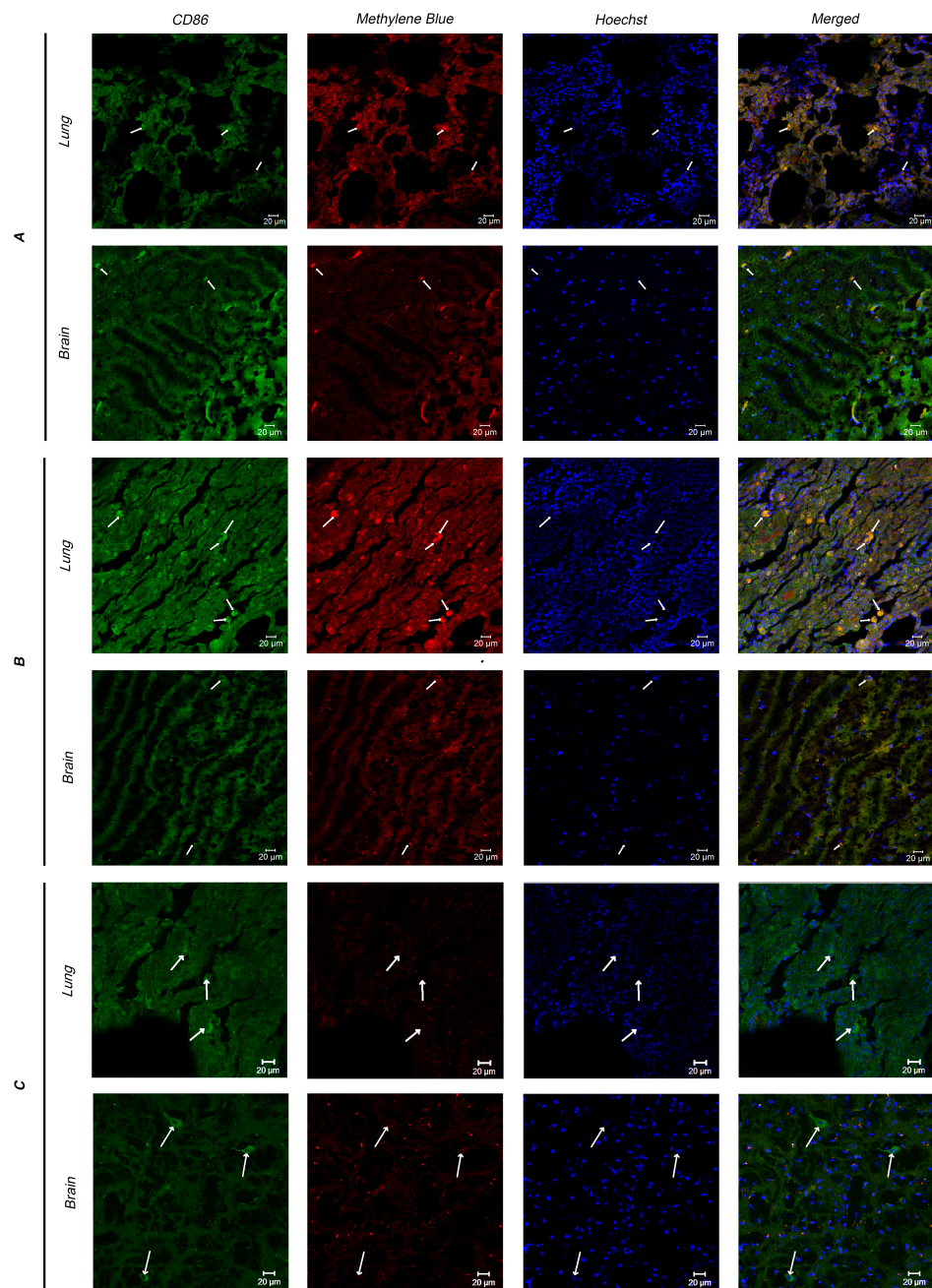


**Figure 12.** Immunofluorescence analysis of lung and brain tissues of three primates ((**A**)—3 h after MB administration, (**B**)—24 h after MB administration, (**C**)—control). Arrows indicate myeloid cells found in tissues. Immunofluorescence reveals that there are cells (macrophages) in the tissues of the lungs and brain which accumulate MB (red) and express Alexa Fluor 488-conjugated CD86 (green) on their surface. Nuclei are demarcated by Hoechst (Blue). Scale bar 20 μm. A 20 × Plan-Apochromat (NA 0.8) lens was used.

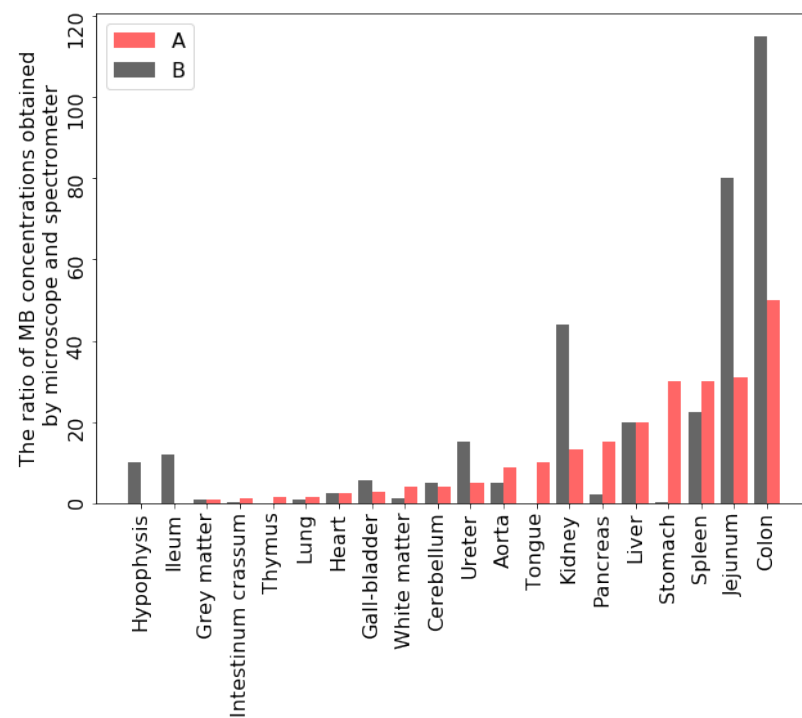


**Figure 13.** The ratio of MB concentrations in different organs obtained by laser scanning confocal microscope and spectrometer: Primate A, 3 h after MB administration; Primate B, 24 h after MB administration.

The MB accumulation in 3 h after oral administration in the thin layer is much greater than in the volume with the integral assessment method. The MB accumulation after 24 h in the thin layer also exceeds the value obtained in the volume of tissues with the exception of the colon and stomach. From these tissues, some of the MB is washed out in a formalin solution during fixation. It can be assumed that in vivo MB elimination from them will be the fastest compared to other organs. This makes it possible to consider the concentration accumulated in these organs as a reference concentration for further determining the required dose and the frequency of drug intake to maintain a constant therapeutic concentration of MB in the organs of patients.

#### 4. Discussion

Previously, Peter C. et al. carried out a comparative study of two different types of administration, followed by an assessment of the MB accumulation in rats, where the differences in pharmacokinetics after oral and intravenous administration within five organs were noted [19]. Zhi-guang Tian and colleagues showed in a rat model that MB alleviated paraquat-induced histological damage, and the administration of MB significantly increased the activity of superoxide dismutase and decreased wet-to-dry lung weight ratio and may be used as a new therapy in the treatment of paraquat-induced acute lung injury [30]. It is also possible that in lung tissues as well as in different organs MB transforms to the colorless form, LMB, so the fluorescence signal is lower. Registration of reduced MB form is of great interest and should be performed for example by liquid chromatography. In addition, there is one new clinical trial, in which MB administration was performed by inhalation [31]. This administration method may be preferable in the event of severe lung damage due to a higher accumulation of MB in lung tissues than by oral administration. However, the MB accumulation by various tissue types, as well as by immune cells, was not previously studied on primates or humans.

Using a scanning laser confocal microscope, it is possible to more accurately determine the concentration of the administered drug in endothelial tissues, which is more promising for further control of viral diseases, the particles of which primarily affect the cells of the

surface layer of organs. For example, the tendency of MB to mainly accumulate in the inner layers of the intestinal tract can give an advantage in the treatment of COVID-19.

The use of a fiber-optic spectrometer enables rapid intraoperative control over the MB accumulation in various organs.

The immunofluorescence analysis showed the presence of myeloid cells in the tissues of the lungs and brain, as well as their accumulation of MB. This fact indicates the possibility of deactivating immunocompetent cells—monocytes and macrophages—which participate in the pathological autoimmune reaction, using light radiation of the red spectral range due to the photodynamic effect in the treatment of viral and oncological diseases.

## 5. Conclusions

The paper presents data on the interstitial distribution of MB at both macro- and microlevels after oral administration of the drug to primates of the *Hamadryas* baboons species, obtained using spectral-fluorescent methods of analysis.

This approach to the analysis of the MB distribution in tissues demonstrates that the MB accumulation in the endothelial layer is significantly higher than in the volume of the tissues. This fact is significant since SARS-CoV-2 attacks endothelial cells via ACE2 receptors.

Using immunofluorescence analysis, it was shown that the accumulation occurs in myeloid cells, which can lead to the inhibition of the pathological autoimmune response during COVID-19. This fact also suggests the possibility of macrophage repolarization into a pro-inflammatory phenotype.

In this work, an emphasis was placed on the MB distribution in all types of tissues of primates and its accumulation in myeloid cells. However, the properties of MB and LMB are not limited to this and require further study.

**Author Contributions:** Project administration, E.I.K.; Writing—review and editing, E.I.K.; Visualization, E.I.K.; Methodology, D.V.P. and A.V.R.; Formal analysis, K.T.E.; Investigation, K.T.E., A.V.R., A.S.S., N.S.R., E.I.M., O.G.K. and G.A.Z.; Resources, D.V.B., D.D.K. and A.A.S.; Supervision, I.V.R. and V.B.L. All authors have read and agreed to the published version of the manuscript.

**Funding:** This work was supported by RFBR, 20-04-60421.

**Institutional Review Board Statement:** The study was conducted according to the guidelines of the Declaration of Helsinki, and approved by the Institutional Ethics Committee of Research Institute of Medical Primatology (protocol No. 57, 21 November 2020). Three hamadryas baboons (*Papio hamadryas*) were involved in this study. All animals were separated in a conventional environment at the Experimental Animal Center of Research Institute of Medical Primatology. The animals were free to drink water and were fed two times a day with standard diet. The team consists of the anesthetist, veterinarian, and nurse, who managed the drug use during the experiment. All animals were closely monitored by the researcher and animal care staff throughout the day. The day after the experiment, the animals were sacrificed.

**Informed Consent Statement:** Not applicable.

**Data Availability Statement:** The authors confirm that the data supporting the findings of this study are available within the article.

**Conflicts of Interest:** The authors declare no conflict of interest.

## References

1. Auerbach, S.S.; Bristol, D.W.; Peckham, J.C.; Travlos, G.S.; Hébert, C.D.; Chhabra, R.S. Toxicity and carcinogenicity studies of methylene blue trihydrate in F344N rats and B6C3F1 mice. *Food Chem. Toxicol.* **2010**, *48*, 169–177. [[CrossRef](#)] [[PubMed](#)]
2. Ginimuge, P.R.; Jyothi, S. Methylene blue: Revisited. *J. Anaesthesiol. Clin. Pharmacol.* **2010**, *26*, 517–520.
3. Wendel, W.B. The control of methemoglobinemia with methylene blue. *J. Clin. Investig.* **1939**, *18*, 179–185. [[CrossRef](#)] [[PubMed](#)]
4. Schirmer, R.H.; Coulibaly, B.; Stich, A.; Scheiwein, M.; Merkle, H.; Eubel, J.; Becker, K.; Becher, H.; Müller, O.; Zich, T.; et al. Methylene blue as an antimalarial agent. *Redox Rep.* **2003**, *8*, 272–275. [[CrossRef](#)]
5. Oz, M.; Lorke, D.E.; Petroianu, G.A. Methylene blue and Alzheimer's disease. *Biochem. Pharmacol.* **2009**, *78*, 927–932. [[CrossRef](#)] [[PubMed](#)]
6. Atamna, H.; Kumar, R. Protective role of methylene blue in Alzheimer's disease via mitochondria and cytochrome c oxidase. *J. Alzheimer's Dis.* **2010**, *20*, S439–S452. [[CrossRef](#)] [[PubMed](#)]

7. Bradberry, S.M. Occupational methaemoglobinaemia. *Toxicol. Rev.* **2003**, *22*, 13–27. [[CrossRef](#)]
8. Hamel, J. A review of acute cyanide poisoning with a treatment update. *Crit. Care Nurse* **2011**, *31*, 72–82. [[CrossRef](#)] [[PubMed](#)]
9. Moody, J.; Allan, S.; Smith, A.; Naylor, G. Methylene blue excretion in depression. *Biol. Psychiatry* **1989**, *26*, 850–852. [[CrossRef](#)]
10. Gillman, P. Methylene blue implicated in potentially fatal serotonin toxicity. *Anaesthesia* **2006**, *61*, 1013–1014. [[CrossRef](#)]
11. Cwalinski, T.; Polom, W.; Marano, L.; Roviello, G.; D'Angelo, A.; Cwalina, N.; Matuszewski, M.; Roviello, F.; Jaskiewicz, J.; Polom, K. Methylene Blue—Current Knowledge, Fluorescent Properties, and Its Future Use. *J. Clin. Med.* **2020**, *9*, 3538. [[CrossRef](#)]
12. Zhang, C.; Jiang, D.; Huang, B.; Wang, C.; Zhao, L.; Xie, X.; Zhang, Z.; Wang, K.; Tian, J.; Luo, Y. Methylene blue-based near-infrared fluorescence imaging for breast cancer visualization in resected human tissues. *Technol. Cancer Res. Treat.* **2019**, *18*, 1533033819894331. [[CrossRef](#)] [[PubMed](#)]
13. Jiang, L.; Liu, T.; Wang, X.; Li, J.; Zhao, H. Real-time near-infrared fluorescence imaging mediated by blue dye in breast cancer patients. *J. Surg. Oncol.* **2020**, *121*, 964–966. [[CrossRef](#)] [[PubMed](#)]
14. Dos Santos, A.F.; Terra, L.F.; Wailemann, R.A.; Oliveira, T.C.; de Moraes Gomes, V.; Mineiro, M.F.; Meotti, F.C.; Bruni-Cardoso, A.; Baptista, M.S.; Labriola, L. Methylene blue photodynamic therapy induces selective and massive cell death in human breast cancer cells. *BMC Cancer* **2017**, *17*, 194. [[CrossRef](#)]
15. Tardivo, J.P.; Del Giglio, A.; De Oliveira, C.S.; Gabrielli, D.S.; Junqueira, H.C.; Tada, D.B.; Severino, D.; de Fátima Turchiello, R.; Baptista, M.S. Methylene blue in photodynamic therapy: From basic mechanisms to clinical applications. *Photodiagnosis Photodyn. Ther.* **2005**, *2*, 175–191. [[CrossRef](#)]
16. Eickmann, M.; Gravemann, U.; Handke, W.; Tolksdorf, F.; Reichenberg, S.; Müller, T.H.; Seltsam, A. Inactivation of Ebola virus and Middle East respiratory syndrome coronavirus in platelet concentrates and plasma by ultraviolet C light and methylene blue plus visible light, respectively. *Transfusion* **2018**, *58*, 2202–2207. [[CrossRef](#)]
17. Jin, C.; Yu, B.; Zhang, J.; Wu, H.; Zhou, X.; Yao, H.; Liu, F.; Lu, X.; Cheng, L.; Jiang, M.; et al. Methylene blue photochemical treatment as a reliable SARS-CoV-2 plasma virus inactivation method for blood safety and convalescent plasma therapy for the COVID-19 outbreak. *BMC Infect. Dis.* **2021**, *21*, 357.
18. Henry, M.; Summa, M.; Patrick, L.; Schwartz, L. A cohort of cancer patients with no reported cases of SARS-CoV-2 infection: The possible preventive role of Methylene Blue. *Substantia* **2020**, *4*, 888.
19. Peter, C.; Hongwan, D.; Küpfer, A.; Lauterburg, B. Pharmacokinetics and organ distribution of intravenous and oral methylene blue. *Eur. J. Clin. Pharmacol.* **2000**, *56*, 247–250. [[CrossRef](#)]
20. Ramsay, R.; Dunford, C.; Gillman, P. Methylene blue and serotonin toxicity: Inhibition of monoamine oxidase A (MAO A) confirms a theoretical prediction. *Br. J. Pharmacol.* **2007**, *152*, 946–951. [[CrossRef](#)]
21. Lee, S.K.; Mills, A. Novel photochemistry of leuco-Methylene Blue. *Chem. Commun.* **2003**, 2366–2367. [[CrossRef](#)]
22. Wen, Y.; Li, W.; Poteet, E.C.; Xie, L.; Tan, C.; Yan, L.J.; Ju, X.; Liu, R.; Qian, H.; Marvin, M.A.; et al. Alternative mitochondrial electron transfer as a novel strategy for neuroprotection. *J. Biol. Chem.* **2011**, *286*, 16504–16515. [[CrossRef](#)]
23. McDonagh, E.M.; Bautista, J.M.; Youngster, I.; Altman, R.B.; Klein, T.E. PharmGKB summary: Methylene blue pathway. *Pharmacogenetics Genom.* **2013**, *23*, 498. [[CrossRef](#)] [[PubMed](#)]
24. Ahn, H.; Kang, S.G.; Yoon, S.i.; Ko, H.J.; Kim, P.H.; Hong, E.J.; An, B.S.; Lee, E.; Lee, G.S. Methylene blue inhibits NLRP3, NLRC4, AIM2, and non-canonical inflammasome activation. *Sci. Rep.* **2017**, *7*, 12409. [[CrossRef](#)]
25. FDA. 2017. Proveyblue Label. Available online: [https://www.accessdata.fda.gov/drugsatfda\\_docs/label/2017/204630s005lbl.pdf](https://www.accessdata.fda.gov/drugsatfda_docs/label/2017/204630s005lbl.pdf) (accessed on 16 June 2021).
26. Alamdari, D.H.; Moghaddam, A.B.; Amini, S.; Keramati, M.R.; Zarmehri, A.M.; Alamdari, A.H.; Damsaz, M.; Banpour, H.; Yarahmadi, A.; Koliakos, G. Application of methylene blue -vitamin C-N-acetyl cysteine for treatment of critically ill COVID-19 patients, report of a phase-I clinical trial. *Eur. J. Pharmacol.* **2020**, *885*, 173494. [[CrossRef](#)] [[PubMed](#)]
27. Ticino, F.E. Evaluation of the Efficacy of Methylene Blue Administration in SARS-CoV2- Affected Patients: A Phase 2, Randomized, Placebo- Controlled, Single Blind Clinical Trial. Available online: <https://clinicaltrials.gov/ct2/show/NCT04635605> (accessed on 23 July 2021)
28. Bojadzic, D.; Alcazar, O.; Buchwald, P. Methylene Blue Inhibits the SARS-CoV-2 Spike–ACE2 Protein-Protein Interaction—A Mechanism that can Contribute to its Antiviral Activity Against COVID-19. *Front. Pharmacol.* **2020**, *11*, 2255.
29. Shin, J.W.; Seol, I.C.; Son, C.G. Interpretation of animal dose and human equivalent dose for drug development. *J. Korean Med.* **2010**, *31*, 1–7.
30. Tian, Z.G.; Ji, Y.; Yan, W.J.; Xu, C.Y.; Kong, Q.Y.; Han, F.; Zhao, Y.; Pang, Q.F. Methylene blue protects against paraquat-induced acute lung injury in rats. *Int. Immunopharmacol.* **2013**, *17*, 309–313. [[CrossRef](#)] [[PubMed](#)]
31. I.M. Sechenov First Moscow State Medical University. The Clinical Trial of Methylene Blue Application Combined with Photodynamic Therapy for Treatment of SARS-CoV-2 Infected Patients. Available online: <https://clinicaltrials.gov/ct2/show/NCT04933864> (accessed on 23 July 2021).